Article

Structure

Crystal Structure of a Heterotetrameric Katanin p60:p80 Complex

Highlights

- We identified mutations that enhance katanin p60:p80 heterotetramer formation
- We determined the crystal structure of a p60:p80 heterotetramer
- The structure revealed a domain-swapped heterotetramer of two p60:p80 heterodimers
- We showed that different katanin oligomers possess distinct functional properties

Authors

Lenka Faltova, Kai Jiang, Daniel Frey, ..., Anna Akhmanova, Michel O. Steinmetz, Richard A. Kammerer

Correspondence

a.akhmanova@uu.nl (A.A.), michel.steinmetz@psi.ch (M.O.S.), richard.kammerer@psi.ch (R.A.K.)

In Brief

Katanin is a microtubule-severing enzyme that is crucial for many cellular processes. Here, we characterized a tetrameric form of katanin using structural and functional methods. We show that increased tetramerization of katanin affects microtubule binding and severing, suggesting the existence of different katanin forms that possess distinct functional properties.

Faltova et al., 2019, Structure *27*, 1375–1383
September 3, 2019
https://doi.org/10.1016/j.str.2019.07.002

CellPress

Structure
Article

Crystal Structure of a Heterotetrameric Katanin p60:p80 Complex

Lenka Faltova,[1,6] Kai Jiang,[2,3,4,6] Daniel Frey,[1] Yufan Wu,[1] Guido Capitani,[1] Andrea E. Prota,[1] Anna Akhmanova,[2,*] Michel O. Steinmetz,[1,5,*] and Richard A. Kammerer[1,7,*]

[1]Laboratory of Biomolecular Research, Division of Biology and Chemistry, Paul Scherrer Institut, 5232 Villigen PSI, Switzerland
[2]Cell Biology, Department of Biology, Faculty of Science, Utrecht University, Padualaan 8, 3584 CH Utrecht, the Netherlands
[3]The State Key Laboratory Breeding Base of Basic Science of Stomatology (Hubei-MOST) & Key Laboratory of Oral Biomedicine Ministry of Education, School & Hospital of Stomatology, Wuhan University, Wuhan 430071, China
[4]Medical Research Institute, Wuhan University, Wuhan 430071, China
[5]Biozentrum, University of Basel, 4056 Basel, Switzerland
[6]These authors contributed equally
[7]Lead Contact
*Correspondence: a.akhmanova@uu.nl (A.A.), michel.steinmetz@psi.ch (M.O.S.), richard.kammerer@psi.ch (R.A.K.)
https://doi.org/10.1016/j.str.2019.07.002

SUMMARY

Katanin is a microtubule-severing enzyme that is crucial for many cellular processes. Katanin consists of two subunits, p60 and p80, that form a stable complex. The interaction between subunits is mediated by the p60 N-terminal microtubule-interacting and -trafficking domain (p60-MIT) and the p80 C-terminal domain (p80-CTD). Here, we performed a biophysical characterization of the mouse p60-MIT:p80-CTD heterodimer and show that this complex can assemble into heterotetramers. We identified two mutations that enhance heterotetramer formation and determined the X-ray crystal structure of this mutant complex. The structure revealed a domain-swapped heterotetramer consisting of two p60-MIT:p80-CTD heterodimers. Structure-based sequence alignments suggest that heterotetramerization of katanin might be a common feature of various species. Furthermore, we show that enhanced heterotetramerization of katanin impairs its microtubule end-binding properties and increases the enzyme's microtubule lattice binding and severing activities. Therefore, our findings suggest the existence of different katanin oligomers that possess distinct functional properties.

INTRODUCTION

Microtubules (MTs) are dynamic filamentous cytoskeletal structures that are involved in many fundamental biological processes such as cell division, development, organization of intracellular transport, and ciliary motility (Akhmanova and Steinmetz, 2015; Roll-Mecak, 2019). Many different proteins have been identified that bind either to MT ends or along MT lattices and affect the stability of the MT polymer (Akhmanova and Steinmetz, 2015). Katanin, spastin, and fidgetin are closely related MT-severing enzymes that can catalyze the removal of αβ-tubulin heterodimers from MTs, resulting in the breakage of MTs into shorter fragments. They belong to the ATPase associated with various cellular activities (AAA) protein family (Roll-Mecak and McNally, 2010; Sharp and Ross, 2012). MT-severing enzymes play important roles in many crucial cellular processes, including cell division, cilia biogenesis, and neurite outgrowth (Ahmad et al., 1999; McNally and Roll-Mecak, 2018; McNally et al., 2006; Roll-Mecak and Vale, 2005; Sharma et al., 2007).

Katanin, the first discovered MT-severing enzyme (Hartman et al., 1998), localizes to spindle poles during mitosis in most animal cells and plays a pivotal role in spindle organization (McNally and McNally, 2011; McNally et al., 2014; Srayko et al., 2000). It has been identified as a crucial regulator of early embryonic development, and recessive mutations or deletions in the KATNB1 gene cause severe microcephaly or microlissencephaly (Hu et al., 2014; Mishra-Gorur et al., 2014). Moreover, katanin plays an important role in plants, where it is required for the bending of the plant axis toward the light source (Lindeboom et al., 2013).

We have recently shown that katanin forms a complex with another microcephaly-associated protein, ASPM (abnormal spindle-like microcephaly-associated) (Jiang et al., 2017). Our findings indicate that the katanin:ASPM complex controls spindle pole organization, poleward spindle flux, and spindle positioning, processes that when misregulated could perturb proliferation of neuronal progenitors and lead to microcephaly. Katanin also interacts with CAMSAPs (calmodulin-regulated spectrin-associated proteins) and is required for limiting the length of CAMSAP-bound MT minus-end stretches during interphase (Jiang et al., 2014, 2018).

Katanin is composed of two subunits, p60 and p80. The p60 subunit consists of an N-terminal MT-interacting and trafficking domain (p60-MIT), which is followed by a linker and a C-terminal ATPase domain that possesses the catalytic activity (Figure 1A). The p80 subunit contains an N-terminal WD40 domain and a C-terminal domain (p80-CTD), which are connected by a proline-rich region (Hartman et al., 1998; Roll-Mecak and McNally, 2010). We recently showed that the interaction between katanin subunits is mediated by p80-CTD and p60-MIT that form a stable heterodimeric complex (Jiang et al., 2017; Rezabkova et al., 2017).

Most AAA ATPases are thought to function as hexameric ring complexes. In experiments with purified proteins, the wild-type

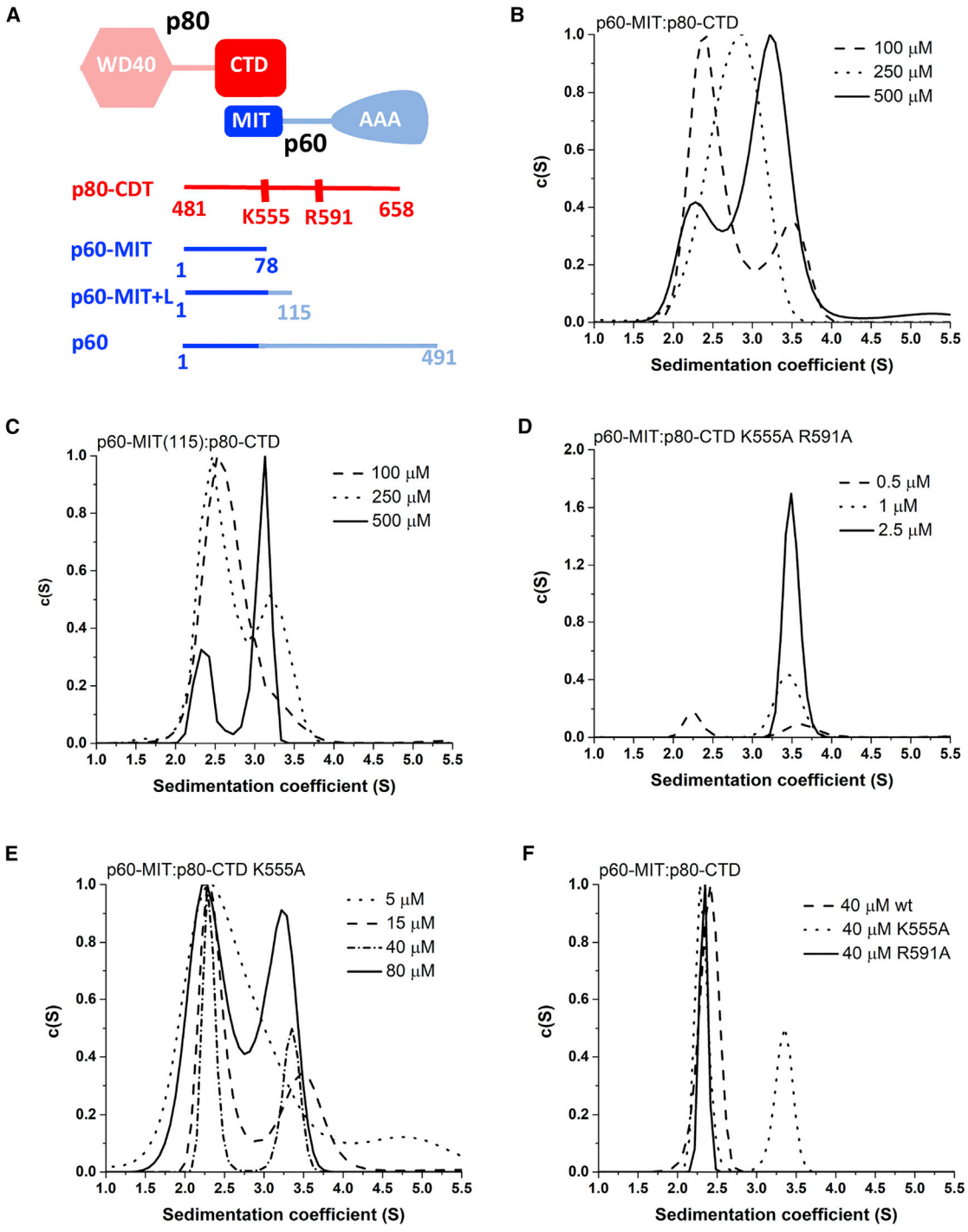

Figure 1. The p60-MIT:p80-CTD Complex Can Form Tetramers at High Protein Concentrations

(A) Schematic representation of the katanin fragments used in this study.

(B–F) c(S) distribution analysis. (B) At concentrations above 100 μM, the p60-MIT:p80-CTD complex shows two peaks in the c(S) distribution, suggesting that the p60-MIT:p80-CTD complex can further assemble into heterotetramers. (C) The p60-MIT (aa 1–115):p80-CTD complex does not show any significant differences in K_D of heterotetramerization compared with the slightly smaller p60-MIT (aa 1–78):p80-CTD complex. (D) p60-MIT:p80-CTD K555A, R591A shows a 500-fold increase in the K_D of heterotetramerization from 250 μM to 500 nM upon introducing two mutations in p80-CTD. (E) Substitution of K555 by A of p80-CTD increases the K_D of heterotetramerization of p60-MIT:p80-CTD K555A approximately 4-fold. (F) In contrast to the K555A mutation, replacing R591 by A has no effect on the K_D of heterotetramerization.

p60 katanin subunit is predominantly monomeric in solution in the absence of ATP; stable hexamers form only upon addition of ATP and binding to MTs (Hartman and Vale, 1999). Recently, several X-ray crystal structures of the monomeric *Caenorhabditis elegans* and human AAA katanin subunit and the cryoelectron microscopy (cryo-EM) structure of the katanin hexamer from *C. elegans* were reported (Nithianantham et al., 2018; Shin et al., 2019; Zehr et al., 2017). The data suggest that katanin cycles between open spiral and closed ring conformations, depending on ATP occupancy (Zehr et al., 2017). Nithianantham et al. reconstituted complexes consisting of full-length p60 and p80-CTD of human katanin and showed that in solution the p60:p80-CTD complex forms not only heterodimers but also heterotetramers (Nithianantham et al., 2018). Previously, heterotetramer formation has also been reported for *C. elegans* MEI-1/MEI-2 katanin (Joly et al., 2016). Although heterotetramer formation is expected to influence hexamerization of p60:p80 heterodimers, its functional significance remains to be investigated.

Here, we performed a biophysical characterization of the heterodimeric mouse katanin p60-MIT:p80-CTD complex (Figure 1A) and confirmed that it can assemble into heterotetramers. We identified two p60-MIT:p80-CTD heterotetramer-enhancing mutations and solved the high-resolution X-ray crystal structure of the mutant complex. Furthermore, we show by functional studies that heterotetramerization of katanin impairs its MT end-binding properties but enhances the enzyme's MT lattice binding and severing activities. Our findings suggest the existence of different oligomeric katanin forms with distinct functional properties.

RESULTS

p60-MIT and p80-CTD Form a Stable Heterodimeric Complex that Can Further Assemble into Heterotetramers

The N-terminal MIT domain of the p60 subunit (p60-MIT, amino acids (aa) 1–78) forms a stable functional complex with the C-terminal domain of the p80 subunit (p80-CTD, aa 481–658) (Jiang et al., 2017; Rezabkova et al., 2017) (Figure 1A). Our previous sedimentation velocity analytical ultracentrifugation (SV-AUC) experiments revealed that p60-MIT and p80-CTD form a heterodimer in the 300-nM to 50-μM concentration range with a sedimentation coefficient, s_w, of 2.4 S and an estimated apparent equilibrium dissociation constant, K_D, in the low nano- to picomolar range (Rezabkova et al., 2017). Surprisingly, at concentrations above 100 μM, a second peak with an s_w value of 3.4 S was observed (Figure 1B), suggesting that p60-MIT and p80-CTD can form heterotetramers with a K_D of approximately 250 μM.

It should be noted in this context that based on a previous nuclear magnetic resonance study, p60-MIT could be potentially involved in heterotetramerization. Iwaya et al. (2006) found that a slightly longer p60-MIT domain (aa 1–90), which contains the linker region (Figure 1A) but not the minimal p60-MIT domain (aa 1–72), can dimerize in solution at a concentration of 40 μM (Iwaya et al., 2006). To assess whether the extra amino acids at the C terminus of the p60-MIT domain have an impact on katanin heterotetramerization, we performed SV-AUC experiments with a complex consisting of p60-MIT (aa 1–115) and p80-CTD. Even at concentrations of up to 500 μM we were not able to detect any significant differences in K_D for p60-MIT (aa 1–115):p80-CTD when compared with p60-MIT (aa 1–78):p80-CTD (Figure 1C), suggesting that the linker has no effect on the heterotetramerization of the mouse katanin complex.

Interestingly, while screening for mutations affecting the interaction of katanin with MTs (Jiang et al., 2017), we identified two single-residue mutations in p80-CTD, K555A, and R591A, which, when introduced together, reduced the K_D of heterotetramerization 500-fold from 250 μM to 500 nM (Figure 1D). The K_D of heterotetramerization of the individual K555A mutant was approximately 4-fold lower (~80 μM) than that of the wild-type protein (Figure 1E), while the R591A mutation alone did not have any effect on the K_D (Figure 1F).

Taken together, the p60-MIT and p80-CTD domains of katanin form a strong heterodimeric complex that can further assemble into heterotetramers. Two mutations were identified, which significantly enhance katanin heterotetramerization.

Crystal Structure of the Heterotetrameric p60-MIT:p80-CTD Complex

We previously determined the crystal structure of the p60-MIT:p80-CTD heterodimer alone (Rezabkova et al., 2017) and in complex with the binding regions of ASPM (Jiang et al., 2017) or CAMSAP (Jiang et al., 2018), two proteins that interact with katanin. In brief, the p60 domain folds into the characteristic antiparallel three-helix bundle that is seen in other MIT domain high-resolution structures. p80-CTD forms an extended helix-turn-helix fold, which consists of seven helices. Heterodimer formation is established through the interaction of the N-terminal helix of p80-CTD with the groove formed between helices H1 and H3 of p60-MIT. The tight interaction between p60-MIT and p80-CTD can be rationalized by the large total surface area of 2,774 $Å^2$ that is buried upon complex formation. The dimer interface is predominantly formed by a large network of hydrophobic interactions, but the high-affinity interaction between p60-MIT and p80-CTD was shown to be also critically dependent on specific hydrogen bonds. The residues involved in p60-MIT:p80-CTD dimer formation are highly conserved among p60 and p80 subunit homologs, suggesting that the mechanism of katanin heterodimerization is very similar among katanin proteins of different species.

To investigate the molecular details of p60-MIT:p80-CTD heterotetramerization, we crystallized the p60-MIT:p80-CTD K555A R591A complex and collected X-ray diffraction datasets. The structure was determined using the p60-MIT:p80-CTD complex structure as a model for molecular replacement (Rezabkova et al., 2017) and was refined to 2.0-Å resolution with four copies of a 2:2 p60-MIT:p80-CTD K555A R591A complex in the asymmetric unit of the crystal (Table 1). The structure revealed a domain-swapped heterotetramer consisting of two p60-MIT:p80-CTD complexes (Figure 2A). The domain swap resulted from a loop-to-helix transition of the hinge loop connecting the third and fourth helix of p80-CTD. The crystal structures of the heterodimer (Rezabkova et al., 2017) and domain-swapped heterotetramer superimpose well outside of the hinge loop region with a root-mean-square deviation (RMSD) value of 0.5 Å over 144 C_α atoms. The interface between the two heterodimers is

Table 1. p60-MIT:p80-CTD K555A R591A Heterotetramer Data Statistics

	p60-MIT:p80-CTD K555A R591A
Data Collection	
Space group	P1
Cell dimensions	
a, *b*, *c* (Å)	45.5, 57.9, 59.8
α, β, γ (°)	108.3, 101.0, 98.3
Resolution (Å)[a]	43.6–2.0 (2.05–2.00)
No. of reflections	36,696 (2,671)
R_{meas} (%)	4.5 (165.6)
$I/\sigma I$	20.2 (1.3)
$CC_{1/2}$	100 (58.7)
Completeness (%)	97.9 (97.0)
Redundancy	7.0 (7.0)
Refinement	
Resolution (Å)	43.6–2.0
No. of unique reflections	36,685
R_{work}/R_{free} (%)	20.9/22.8
Average *B* factors (Å^2)	
Complex	77.9
Solvent	60.4
Wilson *B* factor	48.3
RMSD from ideality	
Bond length (Å)	0.004
Bond angles (°)	0.538
Ramachandran statistics[b]	
Favored regions (%)	99.35
Allowed regions (%)	0.65
Outliers (%)	0

[a]Highest-resolution shell is shown in parentheses.
[b]As defined by MolProbity.

formed exclusively by p80-CTD with a buried total surface area of 1,554.9 Å^2 (Figure 2B). Twelve hydrogen bonds are seen in the interface involving K525, N548, T580, S584, Q590, N545, D557, T561, and D598 and there are two salt bridges formed between K586 and D598. Major hydrophobic interactions at the interface are mediated by V540, W554, I524, A591, S538, V541, L537, L544, L595, P594, G522, V528, V532, L558, Q565, Y577, L569, T583, L587, K586, T521, T561, and D529. The loop-to-helix transition seen in the crystal structure of the p60-MIT:p80-CTD K555A R591A heterotetramer is favored by the K555A mutation (Figures 1E and 1F). The K555A mutation seems to stabilize an extension of an α helix rather than a bend of the hinge loop connecting the third and fourth helix of p80-CTD (Figure 2C). This observation can be rationalized by the fact that alanine is the amino acid residue with the highest helix propensity in soluble proteins (O'Neil and DeGrado, 1990). The extended α helix binds to the empty pocket of another dimer to form the domain-swapped tetramer. Residue R591 is in close proximity to R591′ of the neighboring p80-CTD chain (Figure 2C), explaining how the R591A mutation further contributes to the stabilization of the domain-swapped heterotetramer by avoiding both clashes and electrostatic repulsion between the side chains of the two arginine residues.

To investigate whether the heterotetrameric interface present in the domain-swapped complex mutant is similar to the one present in the wild-type protein, we introduced a single-residue mutation into p60-MIT:p80-CTD to prevent tetramer formation. To this end, we mutated R591 to glutamic acid to bring as a result of its shorter side chain the two repulsive charges potentially into even closer proximity than in arginine. Indeed, we did not observe any heterotetramer formation for the R591E complex mutant even at very high protein concentrations of up to 500 μM (Figure 2D). We therefore conclude that the interactions present in the domain-swapped structure are similar to those in the wild-type heterotetramer.

In our previous work, we identified two highly conserved residues at the C terminus of p80-CTD, R615 and K618, which are essential for MT end binding and bending in cells (Jiang et al., 2017). In the p60-MIT:p80-CTD heterodimer, these residues are well accessible for MT binding. However, in the p60-MIT:p80-CTD heterotetramer the accessibility of this region is limited, and in particular R615 is shielded by the other p80 component of the complex. As a result, the ability to bind and bend MT ends is likely to be compromised (Figure 2E).

Taken together, the crystal structure of the heterotetrameric katanin complex revealed a domain-swapped dimer of p60-MIT:p80-CTD heterodimers whose interface is formed by the p80-CTD loop region.

Heterotetramerization Impairs the MT End-Binding Activity of Katanin but Enhances MT Lattice Binding and Severing

To investigate the functional significance of katanin heterotetramer formation, we next tested the impact of the single K591E and the double K555A/R591A mutations on the enzyme's interaction with MTs and on its severing activity. The experiments were performed with a heterodimeric complex containing the full-length p60 and p80-CTD (p60:p80-CTD), because our previous work showed that this complex can be efficiently purified and used for *in vitro* MT-severing experiments (Jiang et al., 2017). When tested on stable MTs grown in the presence of the slowly hydrolyzable guanosine triphosphate analog GMPCPP and in the absence of free tubulin, the K555A/R591A mutant showed a 17-fold increase in MT binding compared with wild-type katanin, while the R591E mutant displayed a 2-fold reduction in MT binding (Figures 3A and 3B). In agreement with these data, the K555A/R591A mutant severed GMPCPP-stabilized MTs much faster. It even displayed some severing activity at a concentration of 10 nM, whereas neither the wild-type p60:p80-CTD nor the K591E mutant was able to sever MTs at this low concentration (Figures 3C and 3D). The R591E mutant severed MTs ~2-fold slower, which is consistent with the MT binding data (Figures 3C and 3D).

Next, we compared the behavior of the wild-type and mutant p60:p80-CTD complexes on dynamic MTs in the presence of free tubulin. Our previous work showed that under such conditions, the wild-type p60:p80-CTD complex strongly decorates and bends the growing MT plus ends and minus ends (Jiang et al., 2017). This behavior was not affected by the K591E mutant but was blocked by the K555A/R591A

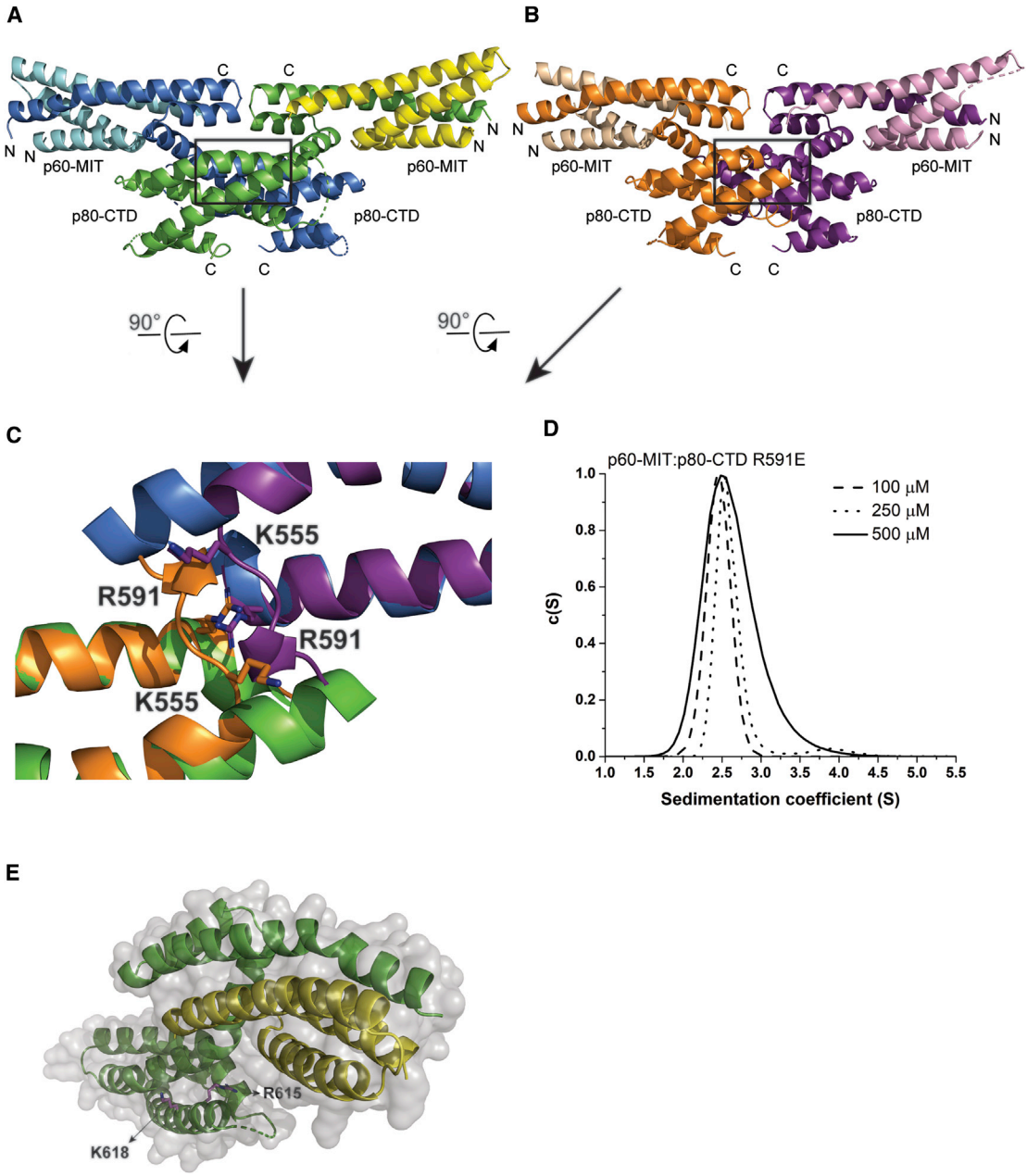

Figure 2. Crystal Structure of the Heterotetrameric p60-MIT:p80-CTD Complex

(A) Ribbon representation of the crystal structure of the domain-swapped p60-MIT:p80-CTD K555A, R591A heterotetrameric complex. p60-MIT is shown in cyan and yellow; p80-CTD is shown in green and blue. N and C termini of p60-MIT and p80-CTD are labeled.

(B) Ribbon representation model of a non-domain-swapped p60-MIT:p80-CTD heterotetrameric complex. p60-MIT is shown in wheat and pink; p80-CTD is shown in orange and purple. N and C termini of p60-MIT and p80-CTD are labeled. p80-CTD residues 550–595 from two biological complexes of wild-type p60-MIT:p80-CTD (PDB: 5NBT) were aligned to the corresponding residues in the domain-swapped p60-MIT:p80-CTD K555A, R591A complex.

(C) Zoom-in view and comparison of the crystal structure of p60-MIT:p80-CTD K555A, R591A heterotetrameric complex shown in ribbon representation with the non-domain-swapped model at the site of the domain swap. K555 and R591 from the model of the non-domain-swapped structure are highlighted as sticks. The color coding is the same as in (A) and (B).

(D) AUC c(S) distributions showing that the R591E mutation prevents tetrameric complex formation even at high protein concentrations.

(E) Cartoon/surface model of the p60-MIT:p80-CTD K555A, R591A heterotetrameric complex structure (chains A and D) rotated 70° along the x axis and −40° along the y axis using the model from (A). The side chains of residues R615 and K618 that are important for MT end binding and bending are colored in magenta and shown as sticks.

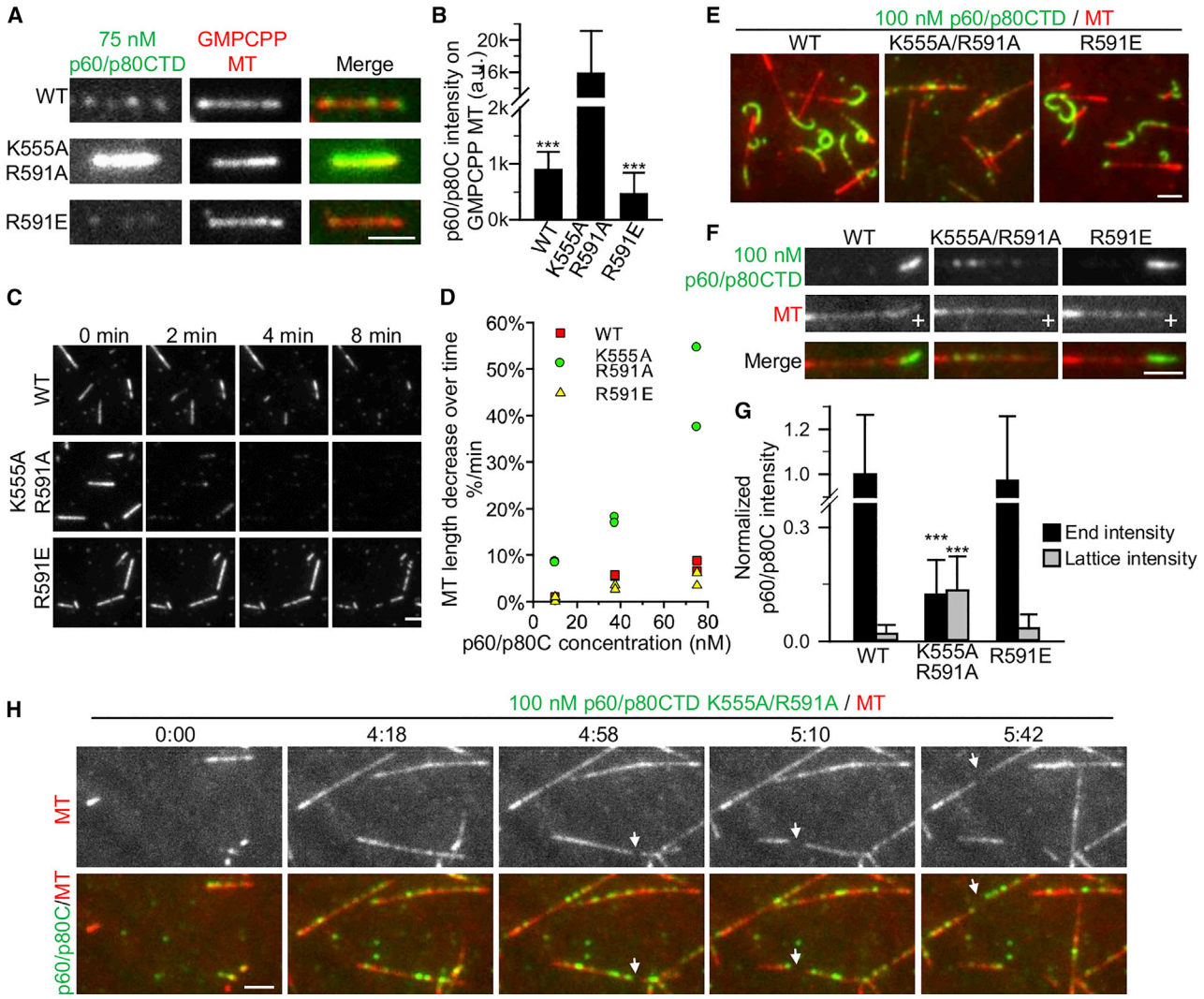

Figure 3. Heterotetramerization of Katanin Impairs MT End Binding and Enhances the Enzyme's MT Lattice Binding and Severing Activities

(A) Total internal reflection fluorescence microscopy (TIRFM) images of wild-type (WT) and mutant (green) p60:SNAP-Alexa 647 p80-CTD complexes localizing to GMPCPP-stabilized MTs, labeled with rhodamine-tubulin (red). Protein concentration, 75 nM. Scale bar, 2 μm.

(B) Quantification of the fluorescence intensity of MT lattice labeling with WT and mutant p60: SNAP-Alexa 647-p80-CTD shown in (A) after background subtraction. Data represent mean ± SD. ***$p < 0.001$, Mann-Whitney U test. Protein concentration, 75 nM; n = 20 MTs in two experiments.

(C) TIRFM time-lapse images of severing of GMPCPP-stabilized MTs, labeled with rhodamine-tubulin by WT and mutant p60:SNAP-Alexa 647-p80-CTD complexes. Protein concentration, 75 nM. Scale bar, 2 μm.

(D) Severing activity of WT and mutant p60:p80-CTD complexes on GMPCPP-stabilized MTs, as shown in (C), at different concentrations. Severing activity was measured as the percentage of MT length decrease over time, relative to the first time point (percent/min). n = 2 experiments.

(E and F) TIRFM images of dynamic MTs, labeled with rhodamine-tubulin grown in the presence of WT and mutant p60:SNAP-Alexa647 p80-CTD complexes. The WT p60:p80-CTD and the R591E mutant can decorate and bend dynamic MT ends, while the K555A/R591A mutant predominantly localizes to the MT lattice. Protein concentration, 100 nM. Scale bar, 2 μm.

(G) Fluorescence intensities of WT and mutant p60/p80-CTD complexes on MT ends and lattices, normalized to the intensity of WT p60/p80-CTD on MT ends. n = 30 MTs in two experiments. Data represent mean ± SD. ***$p < 0.001$, Mann-Whitney U test. Protein concentration, 100 nM.

(H) TIRFM time-lapse images of the p60:p80-CTD K555A/R591A mutant severing dynamic MTs, labeled with rhodamine-tubulin. White arrows indicate severing events. Time represented as minutes:seconds. Protein concentration, 100 nM. Scale bar, 2 μm.

double mutation (Figures 4E–4G). Notably, in the same assays, we observed enhanced binding of the K555A/R591A mutant along dynamic (guanosine diphosphate-bound) MT lattices (Figures 4F and 4G). In agreement with these data, we observed efficient severing of dynamic MTs of p60:p80-CTD K555A/R591A at a concentration of 100 nM (Figure 4H), whereas the wild-type protein, which is strongly inhibited by free tubulin (Bailey et al., 2015), was only able to sever dynamic MTs when present at a concentration of 300 nM (Jiang et al., 2017).

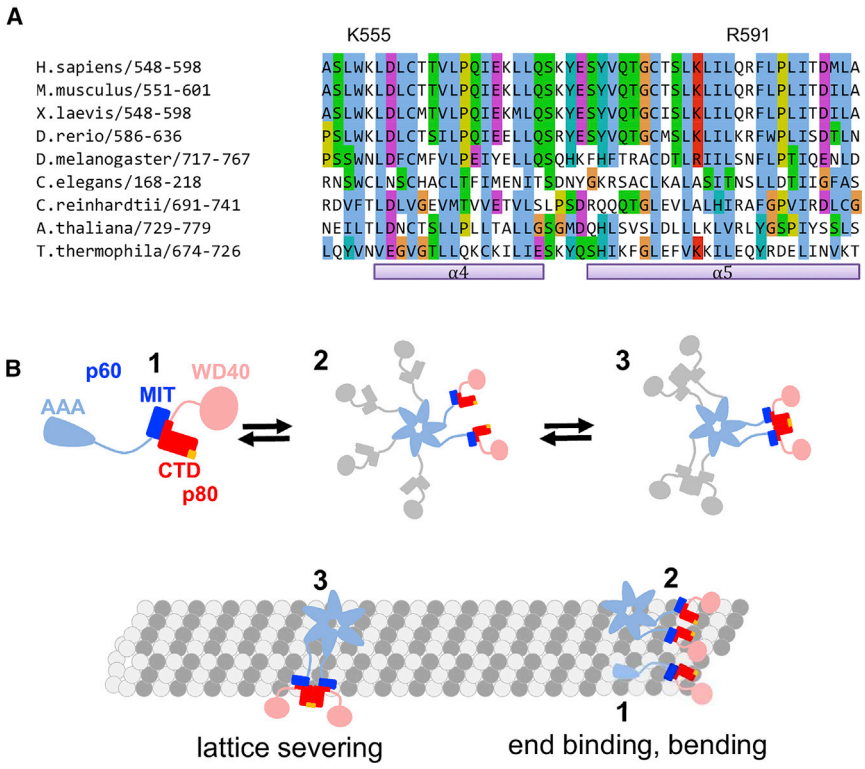

Figure 4. Alignment of Katanin p80 Sequences and Model of Katanin Interactions with MTs

(A) Sequence alignment of katanin p80-CTDs from various species. The mouse residues K555 and R591 are highlighted. The figure was prepared using Jalview (Waterhouse et al., 2009).

(B) The p60MIT:p80-CTD complex might exist in different MT-interacting conformations. Heterodimeric conformations (1 and 2, full-length p60:p80 heterodimer or same dimer in the dodecameric context, respectively) support the binding to curved MT lattices present at growing MT ends. A heterotetrameric conformation (3) promotes binding of katanin to straight MT lattices, formation of the p60 ATPase hexamer, and activation of its MT-severing activity. The p80-CTD region that is important for MT binding is shown in yellow. For clarity concerning MT binding, only two of six of the p60-MIT domains associated with p80 subunits are depicted.

Taken together, enhanced heterotetramerization impairs the MT end-binding activity of katanin and promotes the binding of the enzyme to MTs and its MT-severing activity.

DISCUSSION

In this study, we uncovered an unexpected role of the non-enzymatic p60-MIT and p80-CTD domains of katanin in the oligomerization and regulation of this MT-severing protein. We show that p80-CTD mediates the assembly of p60-MIT:p80-CTD heterodimers into heterotetramers that have an impact on katanin MT end and lattice binding as well as on the severing activity of the enzyme.

The heterotetrameric structure of the p60-MIT:p80-CTD K555A/R591A mutant revealed a domain swap. Domain swapping is defined as the process by which two or more protein molecules exchange a part of their structure to form intertwined oligomers (Rousseau et al., 2003). These domain-swapped oligomers are composed of subunits having the same structure as the original monomer, with the exception of the hinge loop that connects the swapped part with the rest of the protein. In the monomer, the hinge loop typically folds back on itself while it adopts an extended conformation in the domain-swapped oligomer (Rousseau et al., 2003). It has been shown that the K_Ds observed for domain-swapped oligomers for natural proteins are in the micromolar-to-millimolar range (Rousseau et al., 2003). Furthermore, the energy required to increase the interaction is very low: A free energy change of approximately 4 kcal/mol only results in a change in the equilibrium dissociation constant by three orders of magnitude (Rousseau et al., 2003). Thus, a few mutations in the hinge loop and/or in the secondary interface, designed to favor the tetramer, could easily bring the K_D down to the nanomolar range. Accordingly, the two residue mutations in p80-CTD, K555A and R591A, dramatically shift the heterodimer/heterotetramer equilibrium toward the heterotetramer. Based on our findings, we therefore speculate that the domain swap can also occur in the wild-type p60-MIT:p80-CTD complex, where the K_D of heterotetramerization is in the high-micromolar range and the introduction of two single-residue mutations, K555A and R591A, result in a K_D in the nanomolar range. Our conclusion is supported by the p80-CTD R591E mutant, which was designed to bring the two electrostatic repulsive charges in the heterotetramer interface into closer proximity. Consistent with our hypothesis, we did not observe any heterotetramer formation for this particular p80-CTD mutant (Figure 2D).

The heterodimerization of katanin has been previously observed for human and *C. elegans* katanin (Joly et al., 2016; Nithianantham et al., 2018). Nithianantham et al. (2018) reported that human p60:p80-CTD can form tetramers at a concentration around 20 μM while we observed that the heterotetrameric mouse p60-MIT:p80-CTD complex forms at protein concentrations around 100–200 μM. These observations suggest that both the AAA ATPase domain and the p60-MIT:p80-CTD complex contribute to heterotetramerization. Notably, *C. elegans* MEI-1/MEI-2 katanin was found to be exclusively tetrameric (Joly et al., 2016). Consistent with our results, the residues corresponding to K555 and R591 in MEI-2 are cysteine and serine, respectively. Both amino acids are uncharged and contain shorter side chains than lysine and arginine, and therefore resemble more the alanine residue that led to increased heterotetramer formation in our experiments. We therefore speculate that *C. elegans* katanin heterotetramers might also be present in the domain-swapped form. As shown in the sequence alignment in Figure 4A, small and uncharged amino acids instead of arginines and lysines are also found in the p80 subunit of other organisms (Figure 4A). Accordingly,

heterotetramerization of katanin might be a common feature of various species.

Our data have important implications for katanin function. They show that MT end decoration and bending, which depend on the heterodimer of the p80-CTD and p60-MIT with the adjacent linker region (p60MIT+L) (Figure 1A) is incompatible with the heterotetramerization of the p60-MIT:p80-CTD complex. This finding can be rationalized by the crystal structures of heterodimeric and heterotetrameric p60-MIT:p80-CTD complexes. In the p60-MIT:p80-CTD heterodimer, residues R615 and K618, which are required for both MT end association and deformation, are well accessible for MT binding. In the p60-MIT:p80-CTD heterotetramer, however, R615 is not accessible and therefore the ability to bind and bend MT ends is likely to be compromised (Figure 2E). In contrast, MT lattice binding and severing are promoted by the formation of the p60-MIT:p80-CTD heterotetramer. Therefore, we conclude that within katanin, the p60MIT+L:p80-CTD complex could exist in different MT-interacting conformations. Since in our previous experiments we demonstrated that p60MIT+L:p80-CTD is able to decorate and bend dynamic MT ends, one conformation might correspond to a heterodimer of full-length p60 and p80. Alternatively, the heterodimeric p60-MIT:p80-CTD conformation could also be present in the active dodecameric form of katanin. Based on our results, both forms could bind to curved MT lattices present at growing MT ends (Jiang et al., 2017). Our findings indicate that the heterotetrameric form could promote katanin dodecamer formation mediated by the ATPase domain of p60, leading to enhanced MT lattice binding and severing (Figure 4B). As a result of the presence of interactions between AAA domains and between p60-MIT and p80-CTD, the formation of higher-order oligomers consisting of katanin dodecamers also cannot be excluded. Possibly, the different oligomerization states are regulated by the binding partners of katanin.

In summary, our findings on the existence of distinct heterodimeric and heterotetrameric forms within katanin dodecamers contribute toward our understanding of how the enzyme drives many important biological processes.

STAR★METHODS

Detailed methods are provided in the online version of this paper and include the following:

- KEY RESOURCES TABLE
- LEAD CONTACT AND MATERIALS AVAILABILITY
- EXPERIMENTAL MODEL AND SUBJECT DETAILS
- METHODS DETAILS
  - DNA Constructs, Protein Expression and Purification
  - Analytical Ultracentrifugation (AUC)
  - Crystallization and X-ray Structure Determination
  - Protein Expression and Purification from HEK293T Cells
  - *In vitro* MT Binding and Severing Assays
  - Total Internal Reflection Fluorescence (TIRF) Microscopy
  - Image Processing
- QUANTIFICATION AND STATISTICAL ANALYSIS
- DATA AND CODE AVAILABILITY

ACKNOWLEDGMENTS

We thank the beamline scientists at beamline X06DA of the Swiss Light Source (Paul Scherrer Institut, Villigen, Switzerland) for technical assistance with the X-ray data collection. This work was supported by the Netherlands Organisation for Scientific Research ALW Open Program grant 824.15.017 to A.A., the EMBO long-term and Marie Curie IEF fellowships to L.F. (awarded under her maiden name L. Rezabkova) and grants from the Swiss National Science Foundation (31003A_166608 to M.O.S. and 31003A_163449 to R.A.K.).

AUTHOR CONTRIBUTIONS

L.F., K.J., R.A.K., M.O.S., and A.A. designed experiments, analyzed the data, and wrote the paper. L.F. performed the biophysical experiments. K.J. carried out all microtubule *in vitro* experiments. L.F., Y.W., and D.F. produced the proteins. L.F., G.C., and A.E.P. performed crystallization experiments and solved the structure.

DECLARATION OF INTERESTS

The authors declare no competing interests.

Received: July 26, 2018
Revised: May 27, 2019
Accepted: July 5, 2019
Published: July 25, 2019

REFERENCES

Adams, P.D., Afonine, P.V., Bunkóczi, G., Chen, V.B., Davis, I.W., Echols, N., Headd, J.J., Hung, L.-W., Kapral, G.J., Grosse-Kunstleve, R.W., et al. (2010). PHENIX: a comprehensive Python-based system for macromolecular structure solution. Acta Crystallogr. D. Biol. Crystallogr. *66*, 213–221.

Ahmad, F.J., Yu, W., McNally, F.J., and Baas, P.W. (1999). An essential role for katanin in severing microtubules in the neuron. J. Cell Biol. *145*, 305–315.

Akhmanova, A., and Steinmetz, M.O. (2015). Control of microtubule organization and dynamics: two ends in the limelight. Nat. Rev. Mol. Cell Biol. *16*, 711–726.

Bailey, M.E., Sackett, D.L., and Ross, J.L. (2015). Katanin severing and binding microtubules are inhibited by tubulin carboxy tails. Biophys. J. *109*, 2546–2561.

Brown, P.H., Balbo, A., and Schuck, P. (2008). Characterizing protein-protein interactions by sedimentation velocity analytical ultracentrifugation. Curr. Protoc. Immunol., Chapter 18, Unit 18.15.

Emsley, P., Lohkamp, B., Scott, W.G., and Cowtan, K. (2010). Features and development of Coot. Acta Crystallogr. D. Biol. Crystallogr. *66*, 486–501.

Gibson, D.G., Young, L., Chuang, R.-Y., Venter, J.C., Hutchison, C.A., and Smith, H.O. (2009). Enzymatic assembly of DNA molecules up to several hundred kilobases. Nat. Methods *6*, 343–345.

Hartman, J.J., and Vale, R.D. (1999). Microtubule disassembly by ATP-dependent oligomerization of the AAA enzyme katanin. Science *286*, 782–785.

Hartman, J.J., Mahr, J., McNally, K., Okawa, K., Iwamatsu, A., Thomas, S., Cheesman, S., Heuser, J., Vale, R.D., and McNally, F.J. (1998). Katanin, a microtubule-severing protein, is a novel AAA ATPase that targets to the centrosome using a WD40-containing subunit. Cell *93*, 277–287.

Hu, W.F., Pomp, O., Ben-Omran, T., Kodani, A., Henke, K., Mochida, G.H., Yu, T.W., Woodworth, M.B., Bonnard, C., Raj, G.S., et al. (2014). Katanin p80 regulates human cortical development by limiting centriole and cilia number. Neuron *84*, 1240–1257.

Iwaya, N., Goda, N., Unzai, S., Fujiwara, K., Tanaka, T., Tomii, K., Tochio, H., Shirakawa, M., and Hiroaki, H. (2006). Fine-tuning of protein domain boundary by minimizing potential coiled coil regions. J. Biomol. NMR *37*, 53–63.

Jiang, K., Hua, S., Mohan, R., Grigoriev, I., Yau, K., Liu, Q., Katrukha, E.A., Altelaar, A.F., Heck, A.J.R., Hoogenraad, C.C., et al. (2014). Microtubule minus-end stabilization by polymerization-driven CAMSAP deposition. Dev. Cell *28*, 295–309.

Jiang, K., Rezabkova, L., Hua, S., Liu, Q., Capitani, G., Maarten Altelaar, A.F., Heck, A.J.R., Kammerer, R.A., Steinmetz, M.O., and Akhmanova, A. (2017). Microtubule minus-end regulation at spindle poles by an ASPM-katanin complex. Nat. Cell Biol. *19*, 480–492.

Jiang, K., Faltova, L., Hua, S., Capitani, G., Prota, A.E., Landgraf, C., Volkmer, R., Kammerer, R.A., Steinmetz, M.O., and Akhmanova, A. (2018). Structural basis of formation of the microtubule minus-end-regulating CAMSAP-katanin complex. Structure *26*, 375–382.

Joly, N., Martino, L., Gigant, E., Dumont, J., and Pintard, L. (2016). Microtubule-severing activity of the AAA+ ATPase katanin is essential for female meiotic spindle assembly. Development *143*, 3604–3614.

Kabsch, W. (2010a). XDS. Acta Crystallogr. D. Biol. Crystallogr. *66*, 125–132.

Kabsch, W. (2010b). Integration, scaling, space-group assignment and post-refinement. Acta Crystallogr. D. Biol. Crystallogr. *66*, 133–144.

Lindeboom, J.J., Nakamura, M., Hibbel, A., Shundyak, K., Gutierrez, R., Ketelaar, T., Emons, A.M.C., Mulder, B.M., Kirik, V., and Ehrhardt, D.W. (2013). A mechanism for reorientation of cortical microtubule arrays driven by microtubule severing. Science *342*, 1245533.

McNally, F.J., and Roll-Mecak, A. (2018). Microtubule-severing enzymes: from cellular functions to molecular mechanism. J. Cell Biol. *217*, 4057–4069.

McNally, K.P., and McNally, F.J. (2011). The spindle assembly function of Caenorhabditis elegans katanin does not require microtubule-severing activity. Mol. Biol. Cell *22*, 1550–1560.

McNally, K., Audhya, A., Oegema, K., and McNally, F.J. (2006). Katanin controls mitotic and meiotic spindle length. J. Cell Biol. *175*, 881–891.

McNally, K., Berg, E., Cortes, D.B., Hernandez, V., Mains, P.E., and McNally, F.J. (2014). Katanin maintains meiotic metaphase chromosome alignment and spindle structure in vivo and has multiple effects on microtubules in vitro. Mol. Biol. Cell *25*, 1037–1049.

Mishra-Gorur, K., Çağlayan, A.O., Schaffer, A.E., Chabu, C., Henegariu, O., Vonhoff, F., Akgümüş, G.T., Nishimura, S., Han, W., Tu, S., et al. (2014). Mutations in KATNB1 cause complex cerebral malformations by disrupting asymmetrically dividing neural progenitors. Neuron *84*, 1226–1239.

Nithianantham, S., McNally, F.J., and Al-Bassam, J. (2018). Structural basis for disassembly of katanin heterododecamers. J. Biol. Chem. *293*, 10590–10605.

O'Neil, K.T., and DeGrado, W.F. (1990). A thermodynamic scale for the helix-forming tendencies of the commonly occurring amino acids. Science *250*, 646–651.

Rezabkova, L., Jiang, K., Capitani, G., Prota, A.E., Akhmanova, A., Steinmetz, M.O., and Kammerer, R.A. (2017). Structural basis of katanin p60:p80 complex formation. Sci. Rep. *7*, 14893.

Roll-Mecak, A. (2019). How cells exploit tubulin diversity to build functional cellular microtubule mosaics. Curr. Opin. Cell Biol. *56*, 102–108.

Roll-Mecak, A., and McNally, F.J. (2010). Microtubule-severing enzymes. Curr. Opin. Cell Biol. *22*, 96–103.

Roll-Mecak, A., and Vale, R.D. (2005). The *Drosophila* homologue of the hereditary spastic paraplegia protein, spastin, severs and disassembles microtubules. Curr. Biol. *15*, 650–655.

Rousseau, F., Schymkowitz, J.W.H., and Itzhaki, L.S. (2003). The unfolding story of three-dimensional domain swapping. Structure *11*, 243–251.

Schuck, P. (2000). Size-distribution analysis of macromolecules by sedimentation velocity ultracentrifugation and lamm equation modeling. Biophys. J. *78*, 1606–1619.

Sharma, N., Bryant, J., Wloga, D., Donaldson, R., Davis, R.C., Jerka-Dziadosz, M., and Gaertig, J. (2007). Katanin regulates dynamics of microtubules and biogenesis of motile cilia. J. Cell Biol. *178*, 1065–1079.

Sharp, D.J., and Ross, J.L. (2012). Microtubule-severing enzymes at the cutting edge. J. Cell Sci. *125*, 2561–2569.

Shin, S.C., Im, S.K., Jang, E.H., Jin, K.S., Hur, E.M., and Kim, E.E.K. (2019). Structural and molecular basis for katanin-mediated severing of glutamylated microtubules. Cell Rep. *26*, 1357–1367.e5.

Srayko, M., Buster, D.W., Bazirgan, O.A., McNally, F.J., and Mains, P.E. (2000). MEI-1/MEI-2 katanin-like microtubule severing activity is required for Caenorhabditis elegans meiosis. Genes Dev. *14*, 1072–1084.

Waterhouse, A.M., Procter, J.B., Martin, D.M.A., Clamp, M., and Barton, G.J. (2009). Jalview Version 2—a multiple sequence alignment editor and analysis workbench. Bioinformatics *25*, 1189–1191.

Zehr, E., Szyk, A., Piszczek, G., Szczesna, E., Zuo, X., and Roll-Mecak, A. (2017). Katanin spiral and ring structures shed light on power stroke for microtubule severing. Nat. Struct. Mol. Biol. *24*, 717–725.

Zhao, H., Brautigam, C.A., Ghirlando, R., and Schuck, P. (2013). Overview of current methods in sedimentation velocity and sedimentation equilibrium analytical ultracentrifugation. Curr. Protoc. Protein Sci. *71*, 20.12.1–20.12.49.

STAR★METHODS

KEY RESOURCES TABLE

REAGENT or RESOURCE	SOURCE	IDENTIFIER
Bacterial and Virus Strains		
E.Coli BL21 (DE3)	Agilent	200131
Chemicals, Peptides, and Recombinant Proteins		
HisTrap FF, 5 ml column	GE Healthcare	17-5255-01
HiLoad 16/600 Superdex 75 pg column	GE Healthcare	28-9893-33
p60-MIT:p80-CTD	Rezabkova et al. (2017)	N/A
p60-MIT+L:p80-CTD	this paper	N/A
p60-MIT:p80-CTD K555A	this paper	N/A
p60-MIT:p80-CTD R591A	this paper	N/A
p60-MIT:p80-CTD K555A R591A	this paper	N/A
p60-MIT:p80-CTD R591E	this paper	N/A
p60:Strep-SNAP p80-CTD	Jiang et al., (2017)	N/A
p60:Strep-SNAP p80-CTD K555A R591A	this paper	N/A
p60:Strep-SNAP p80-CTD R591E	this paper	N/A
StrepTactin Sepharose High Performance	GE Healthcare	28-9355-99
Polyethylenimine	Polysciences	24765-2
cOmplete™ Protease Inhibitor Cocktail	Roche	4693116001
Tubulin Porcine	Cytoskeleton	T240-C
Tubulin Porcine Rhodamine	Cytoskeleton	TL590M
Tubulin Porcine Biotin	Cytoskeleton	T333P
GMPCPP	Jena Biosciences	NU-405L
GTP	Sigma	G8877
Glucose oxidase	Sigma	G7141
Catalase	Sigma	C9322
DTT	Sigma	R0861
k-casein	Sigma	C0406
Neutravidin	Invitrogen	A-2666
SNAP-Surface® Alexa Fluor® 647	NEB	S9136S
Deposited Data		
Atomic coordinates and structure factors	this paper	PDB:6GZC
Atomic coordinates and structure factors	Jiang et al., (2017)	PDB:5NBT
Experimental Models: Cell Lines		
Human: HEK293T	ATCC	CRL-11268
Software and Algorithms		
OriginPro 2016	OriginLab	www.OriginLab.com
Sedfit	Schuck, 2000	https://sedfitsedphat.nibib.nih.gov/software/default.aspx
XDS	Kabsch, 2010	http://xds.mpimf-heidelberg.mpg.de
Phenix	Adams et al., 2010	https://www.phenix-online.org/documentation/reference/refinement.html
COOT	Emsley et al., 2010	https://www2.mrc-lmb.cam.ac.uk/personal/pemsley/coot/
ImageJ	NIH	https://imagej.nih.gov/ij/
Sigmaplot 12	Systat Software Inc	https://systatsoftware.com/

LEAD CONTACT AND MATERIALS AVAILABILITY

Further information and requests for resources and reagents should be directed to and will be fulfilled by the Lead Contact, Richard A. Kammerer (richard.kammerer@psi.ch).

EXPERIMENTAL MODEL AND SUBJECT DETAILS

We used E.coli BL21 (DE3) cells for recombinant expression of p60-MIT:p80-CTD (+mutants) and p60-MIT+L:p80-CTD for biochemical, biophysical and X-ray crystallography experiments. The cells were cultured standardly in LB media.

HEK293T cells were used for the expression of p60:Strept-SNAP-p80-CTD WT and mutants that were employed for *in vitro* MT binding and severing assays. HEK 293T cells (ATCC, derived from human embryonic kidney) were cultured in DMEM/F10 (1:1) supplemented with 10% FBS and 5 U/ml/ penicillin and 50 μg/ml streptomycin at 37°C with 5% CO_2.

METHODS DETAILS

DNA Constructs, Protein Expression and Purification

p60-MIT:p80-CTD, p60:p80-CTD and the corresponding mutants were cloned, expressed and purified as described previously (Jiang et al., 2017; Rezabkova et al., 2017). Briefly, to co-express p60-MIT (AA 1-78) together with p80-CTD (AA 481-658), the second gene with its own Shine-Dalgarno sequence was inserted after the stop codon of the first gene, so that the two proteins were expressed from the same promoter. All mutants were generated either using the QuickChange protocol or the Gibson assembly reaction (Gibson et al., 2009).

6xHis-p80-CTD/p60-MIT was expressed in the pET28a vector (Novagen). Bacterial cells were lysed by ultrasonication in a buffer containing 50 mM HEPES, pH 7.4, supplemented with 500 mMNaCl, 5 mM 2-mercaptoethanol and 10 mM imidazole. The complex was subsequently purified at 4°C by IMAC on a 5 ml HisTrap FF Crude column (GE Healthcare) according to the manufacturer's instructions. The last purification step included size-exclusion chromatography on a Superdex 75 column in a buffer containing 20 mM HEPES, pH 7.4, supplemented with 150 mMNaCl.

Analytical Ultracentrifugation (AUC)

Sedimentation velocity (SV) experiments were performed at 20°C and 42,000 rpm in 20 mM HEPES, pH 7.4, 150 mM NaCl and 2 mM 2-mercaptoethanol in a Beckman Coulter ProteomeLab XL-I analytical ultracentrifuge using standard protocols (Brown et al., 2008; Zhao et al., 2013). All data were acquired using absorbance (280 and 250 nm) or interference. Data analysis was performed with the SEDFIT software package using a sedimentation coefficient distribution model c(S) (Schuck, 2000). Kd was estimated from the c(S) distributions following the amount of dimer and tetramer formed at each concentration.

Crystallization and X-ray Structure Determination

For crystallization, the p60-MIT:p80-CTD K555A R591A complex in 20 mM HEPES, pH 7.5, supplemented with 150 mM NaCl, was concentrated to 20 mg/ml. Crystals of the p60-MIT:p80-CTD K555A R591A complex grew within a few hours at 20°C using the sitting drop method in 10% PEG 8000, 0.1 M HEPES (7.5), 8% ethylene glycol. For cryo-protection, the reservoir solution was supplemented with 25% ethylene glycol. A native data set was acquired at the beamline X06DA of the Swiss Light Source (Paul Scherer Institut, Villigen, Switzerland) to a resolution of 2 Å. The acquired dataset was reduced, scaled and merged using XDS, XSCALE and XDSCONV (Kabsch, 2010b; 2010a). The p60-MIT:p80-CTD K555A R591A structure was determined by molecular replacement in space group P1 using the p60-MIT L40P:p80-CTD complex heterodimer structure as a template. Structure refinement was carried out with Phenix.refine from the Phenix software suite (Adams et al., 2010). The program COOT was used for manual rebuilding (Emsley et al., 2010). Data and refinement statistics are reported in Data Table 1. The structure was deposited in the PDBe databank under accession codes PDB:6GZC. Molecular graphics and analyses were performed with PyMol (The PyMOL Molecular Graphics System, Version 1.5.0.5. Schrödinger, LLC).

Protein Expression and Purification from HEK293T Cells

To co-purify different katanin complexes, p80-CTD with a Strep-SNAP tag was co-transfected with full-length p60 without any tags. 36 hours post transfection, HEK293T cells from one 15 cm dish were lysed in 900 μl lysis buffer (50 mM HEPES, 300 mM NaCl, 0.5% Triton X-100, pH 7.4) supplemented with Complete inhibitor cocktail (Roche). After removing the cell debris by centrifugation, cell lysates were incubated with 100 μl StrepTactin beads (GE Healthcare) for 45 mins. Beads were washed 4 times with lysis buffer without protease inhibitors and twice with wash buffer (50 mM HEPES, 150 mM NaCl, 0.01% Triton X-100). To label SNAP tagged proteins with the Alexa-647 dye (NEB), 20-40 μM dye diluted in wash buffer was incubated with proteins on beads for 1 hour. After extensive washing, the proteins were eluted in 60 μl elution buffer (50 mM HEPES, 300 mM NaCl, 0.01% Triton X-100, and 2.5 mM desthiobiotin, pH 7.4). All purified proteins were snap frozen in liquid nitrogen and stored at −80°C.

In vitro MT Binding and Severing Assays

In vitro assays with dynamic MTs were performed under the same conditions as described previously (Jiang et al., 2014). Briefly, after functionalizing coverslips by sequentially incubating them with 0.2 mg/ml PLL-PEG-biotin (Susos AG, Switzerland) and 1 mg/ml neutravidin (Invitrogen) in MRB80 buffer, GMPCPP-stabilized MT seeds were attached to coverslips through biotin-neutravidin interactions. Flow chambers were further blocked with 1 mg/ml κ-casein. The reaction mix with katanin proteins (MRB80 buffer supplemented with 20 μM porcine brain tubulin, 0.5 μM rhodamine-tubulin, 50 mM KCl, 1 mM GTP, 1 mM ATP, 0.2 mg/ml κ-casein, 0.1% methylcellulose and oxygen scavenger mix (50 mM glucose, 400 μg/ml glucose oxidase, 200 μg/ml catalase and 4 mM DTT)) was added to the flow chamber after centrifugation. The flow chamber was sealed with vacuum grease, and dynamic MTs were imaged immediately at 30°C using a TIRF microscope. The conditions for severing assays with GMPCPP-stabilized MTs were the same as in the assays with dynamic MTs except that tubulin was not included in the reaction mix. All tubulin products were from Cytoskeleton.

Total Internal Reflection Fluorescence (TIRF) Microscopy

TIRF microscopy was performed on an inverted research microscope Nikon Eclipse Ti-E (Nikon) with the perfect focus system (PFS) (Nikon) and equipped with the Nikon CFI Apo TIRF 100x 1.49 N.A. oil objective (Nikon), Photometrics Evolve 512 EMCCD (Roper Scientific) or CoolSNAP HQ2 CCD camera (Roper Scientific) and controlled with the MetaMorph 7.7 software (Molecular Devices). Images were projected onto the chip of the Evolve 512 camera with the intermediate lens 2.5X (Nikon C mount adapter 2.5X) or onto CoolSNAP HQ2 without the lens. In both cases the final magnification was 0.063 μm/pixel. To keep *in vitro* samples at 30°C, a INUBG2E-ZILCS stage top incubator (Tokai Hit) was used. For excitation, we used 561 nm 100 mW Jive (Cobolt) and 642 nm 110 mW Stradus (Vortran) lasers. For imaging rhodamine-labelled tubulin and SNAP-Alexa647, the ET-mCherry 49008 (Chroma) and ET-405/488/561/647 filter sets were used. We used sequential acquisition for two colour imaging experiments.

Image Processing

Images were prepared for publication using ImageJ, MetaMorph and Adobe Photoshop. All images were modified by adjustments of levels and contrast. Various quantifications were performed in ImageJ and MetaMorph.

QUANTIFICATION AND STATISTICAL ANALYSIS

All experiments were performed at least twice. Statistical comparison between the data from different groups was performed using Mann-Whitney U test in SigmaPlot.

DATA AND CODE AVAILABILITY

The atomic coordinates and structure factors of the p60-MIT:p80-CTD K555A R591A complex complex have been deposited to the RCSB PDB (www.rcsb.org) with the PDB ID 6GZC.